DEPARTMENT OF PHYSICS

TECHNISCHE UNIVERSITÄT MÜNCHEN

FP 34: Simulating quantum many-body dynamics on a current digital quantum computer

Author:	Franz Von Silva Tarouca
Author:	Christian Gnandt
Author:	Cristian Emiliano Godinez
Supervisor:	Supervisor name
Submission Date:	June 30, 2022

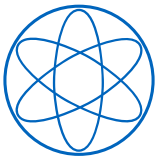

Contents

1 Introduction

The analysis of quantum many-body problems is of utter relevance when aiming to study in depth some of the fundamental quantum mechanical systems. However, in order to do so, it is necessary to deal with the exponential growth in computational resources. Tensor networks have emerged as an ubiquitous tool that can be used to address this challenge.

In this report, we first explain the theory behind the methods here employed such as matrix product state (MPS), time evolution block decimation (TEBD) and dynamic structure factor. With these, the ground state of the Ising model is explored as well as its excited states and the corresponding dynamics such as the time evolution. In addition, these methods allow us to obtain the phase diagram of our Ising hamiltonian with longitudinal and transverse fields as well as the dynamic structure factor.

2 Numerical Methods

2.1 Matrix Product States (MPS)

Within a given Hilbert Space, a random state follows a volume law. In other words, the entanglement entropy of this state grows linearly with the "volume". For a one-dimensional system the "volume" corresponds to the length of the system.

On the other hand, the ground states of a gapped Hamiltonian obey an area law, i.e. the entropy is proportional to the area of the cut that partitions the Hilbert Space. For a 1D case this implies that the entropy is constant with respect to the increase of the system size N.

For the random states mentioned previously, the entanglement entropy is close to its maximum value, for which the Schmidt coefficients are close to being constant. In contrast, the states following an area law (like a ground state) are slightly entangled, which results in most of the weight being distributed in only a few Schmidt coefficients. This subtle but important observation allows for the introduction of a compressed representation of these "product states" known as: matrix-product states (MPS).

We consider a one dimensional chain made up of N sites, with each individual site n having a local basis labeled as $|j_n\rangle$ for $j_n = 0, \dots, d$, where d is the dimension of the nth site's Hilbert Space. The figure below shows a diagrammatic representation of a tensor with N physical legs.

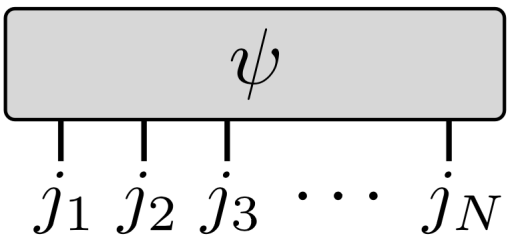

Figure 2.1: Diagram representation of a N dimensional tensor. Source: [1]

The problem is that even for relatively simple configurations, such as a half spin system, an exact

simulation is possible only up to approximately 40 sites [1] due to the exponentially increasing number of entries to store. This is exactly why MPS representation comes in handy. A general pure state can be written in MPS as [1]:

$$|\Psi\rangle = \sum_{j_1,\ldots,j_N} M^{[1]j_1} M^{[2]j_2} \ldots M^{[N]j_N} |j_1, j_2, \ldots, j_N\rangle \tag{2.1}$$

Where each $M^{[n]j_n}$ is a $\chi_n \times \chi_{n+1}$ dimensional matrix and $[n]$ tells us that, for a general state, the matrices on each site could be different. In order to obtain a number as the result of the matrix multiplication, the convention is that $\chi_1 = \chi_{N+1} = 1$, meaning that the first and last matrices are actually vectors.

From the superscript j_n we see that there are d matrices corresponding to each site, and these can be grouped to form a 3-degree tensor as shown here:

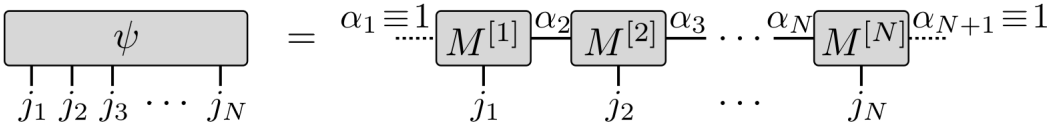

Figure 2.2: MPS representation of quantum state. Source [1]

Where α_i are the virtual legs or bonds, which are by nature different than the physical indices j_n

A so called "canonical form" can be defined based on the freedom of choice of the matrices representing our quantum state. This results in the equation [1]:

$$|\Psi\rangle = \sum_{j_1,\ldots,j_N} \Lambda^{[1]} \Gamma^{[1]j_1} \Lambda^{[2]} \Gamma^{[2]j_2} \Lambda^{[3]} \ldots \Lambda^{[N]} \Gamma^{[N]j_N} \Lambda^{[N+1]} |j_1, j_2, \ldots, j_N\rangle \tag{2.2}$$

Where the matrices $\Lambda^{[n+1]}$ are square diagonal matrices that contain the Schmidt values $\Lambda^{[n+1]}_{\alpha_{n+1}}$ in the diagonal and the $\Gamma^{[n]j_n}$ are such that $\Gamma^{[n]j_n}\Lambda^{[n+1]}$ for each site returns the original state. This grouping, however, can also be done in two different standard ways:

$$A^{[n]j_n} = \Lambda^{[n]}\Gamma^{[n]j_n} \tag{2.3}$$

$$B^{[n]j_n} = \Gamma^{[n]j_n}\Lambda^{[n+1]} \tag{2.4}$$

A state represented solely using matrices of the form given in equation 2.3 is known as **left canonical form**, while one using only matrices of the form in 2.4 is known as **right canonical form**. Mixed representations are also possible.

With this representation, calculating expectation values (of local operators) becomes a relatively easy task. It is useful also to realize that converting from left to right representation (and vice versa) can be readily accomplished by multiplying by the corresponding inverse of the matrix Λ.

2.2 Time Evolving Block Decimation (TEBD)

The time evolving block decimation (TEBD) algorithm allows to calculate the time evolution of a state in MPS representation. This can be done both with a real or imaginary time evolution. The latter can be employed to calculate the ground state using the following relation from [1]:

$$|\psi_{GS}\rangle = \lim_{\tau\to\infty} \frac{e^{-\tau H}|\psi_0\rangle}{||e^{-\tau H}|\psi_0\rangle||} \tag{2.5}$$

Note:
With the help of Trotterization, the time evolution operator can be applied to a state in MPS representation in order to perform a local transformation efficiently. Since local unitaries do not affect the entanglement, the Λ values do not change and thus the amount of information remains the same. This, however, is not the case for two site unitaries like the ones present in our Ising Hamiltonian. Due to this, a cutoff in the Schmidt coefficients ought to be implemented to avoid an exponential grow of information stored.

2.3 Dynamic Structure Factor

The dynamic structure provides information about the excited states of the system under study. In moment and frequency space the dynamic structure for the system of our interest is defined as in [1]:

$$S^{\alpha\alpha}(k,\omega) = \frac{1}{2\pi}\sum_{\mathcal{R}} e^{-ik\cdot\mathcal{R}} \int_{-\infty}^{\infty} e^{i\omega t}\langle\hat{\mathcal{O}}_{\mathcal{R}}^{\alpha\dagger}(t)\hat{\mathcal{O}}_0^{\alpha}(0)\rangle \tag{2.6}$$

To obtain the value of the dynamic structure $S^{\alpha\alpha}$ numerically, it is necessary to discretize the integral (i.e. approximate it by a finite sum) and to allow the time evolution to occur only for a finite time T. The latter results in the lost of information about low frequencies corresponding to small excitations.

In addition, considering only a finite time is equivalent to convoluting the real signal with a square window which results in Gibbs oscillations showing up in the numerical results of $S^{\alpha\alpha}$. To prevent this oscillations from affecting our results, the time series under the Fourier

Transform can be convoluted with a Gaussian window function, resulting in the smoothening of the edges and thus avoiding undesired oscillations.

3 Day 1 – Basics of Matrix Product States

In the following, we will examine a 1D Ising Hamiltonian of the form

$$H = -J \sum_{n=1}^{L} \hat{\sigma}_{\mathrm{x},n} \hat{\sigma}_{\mathrm{x},n+1} - g \sum_{n=1}^{L} \hat{\sigma}_{\mathrm{z},n} - h \sum_{n=1}^{L} \hat{\sigma}_{\mathrm{x},n} \tag{3.1}$$

with L describing the number of lattice sites.

3.1 Single-Site Expectation Values

Initializing our 1-dimensional Ising chain to the all spin-up state (i.e. $|\uparrow\uparrow \ldots \uparrow\rangle \equiv |\Uparrow\rangle$), we obtain the expected expectation values

$$\langle \Uparrow | \hat{\sigma}_{\mathrm{x},i} | \Uparrow \rangle = 0 \tag{3.2}$$

$$\langle \Uparrow | \hat{\sigma}_{\mathrm{z},i} | \Uparrow \rangle = 1 \tag{3.3}$$

for every i, where i is the site on which the operator acts. On the other hand, initializing the state $|\rightarrow\rightarrow \ldots \rightarrow\rangle \equiv |\Rightarrow\rangle$, with $|\rightarrow\rangle = \frac{1}{\sqrt{2}}(|\uparrow\rangle + |\downarrow\rangle)$, we obtain

$$\langle \Rightarrow | \hat{\sigma}_{\mathrm{x},i} | \Rightarrow \rangle = 1 \tag{3.4}$$

$$\langle \Rightarrow | \hat{\sigma}_{\mathrm{z},i} | \Rightarrow \rangle = 0 \tag{3.5}$$

The numerical calculations match these values.

3.2 Energy of 1D Ising Chain

The expectation values of the energy for the states $|\Uparrow\rangle$ and $|\Rightarrow\rangle$ for different values of g are depicted in Fig. 3.1. We see that the energy decreases linearly with increasing g for the $|\Uparrow\rangle$ state, but stays constant for the $|\Rightarrow\rangle$ state. Mathematically, this is the case, because g is a linear coefficient in front of the single site $\hat{\sigma}_{\mathrm{z},i}$-operator. According to the previous section, every site adds $-g$ if the state is $|\Uparrow\rangle$, but does not contribute to the energy if the state is $|\Rightarrow\rangle$.
Physically, the parameter g corresponds to an applied magnetic field in the z-direction. The

anti-alignment of the spins with the magnetic field is energetically favorable. The individual $|\rightarrow\rangle$ states, however, are neither aligned, nor anti-aligned with the field and experience therefore no energy shift. The fact that the $|\Rightarrow\rangle$-state has a lower energy for $g = 0.5$ comes from the fact that $\hat{\sigma}_x$ alignment of nearest neighbors is energetically favorable.

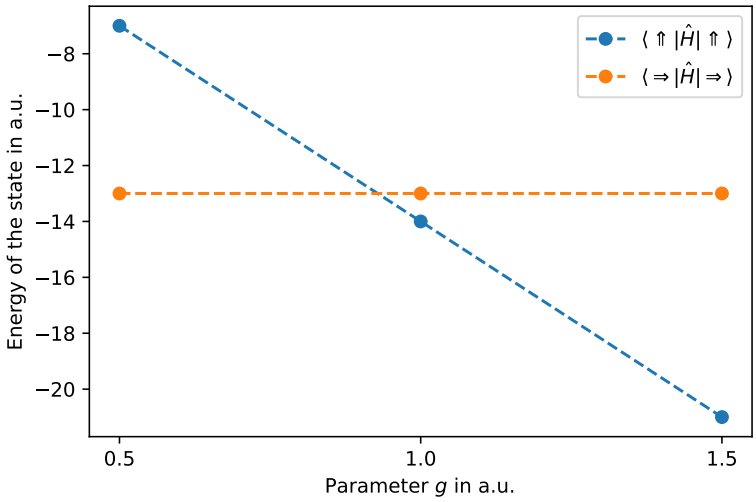

Figure 3.1: Expectation value of the states $|\Uparrow\rangle$ and $|\Rightarrow\rangle$ for a chain length of $L = 14$, $J = 1$ and different values of g.

3.3 Equal-Time Correlations and Magnetization

The equal time correlations $\langle\hat{\sigma}_{x,L/4}\hat{\sigma}_{x,j}\rangle$ for the ground state of the Ising Hamiltonian with $L = 30$, $J = 1$ and different values for g can be seen in Fig. 3.2. For $g \ll 1$, the correlation is roughly constant and approaches 1. For larger values of g we find a linear decrease of the correlations in the logarithmic scaled plot, suggesting an exponential decrease of the correlation. In effect, the magnetic field causes the spins to flip on average, causing a smaller correlation. The downturn for the final values of j is due to the open boundary conditions. Those boundary conditions are also the reason why $L/4$ is used as the reference site.
Using this data, we can extract the magnetization for different values of g. For the magnetization, the following realtion holds:

$$\langle\hat{\sigma}_{x,i}\hat{\sigma}_{x,j}\rangle \rightarrow m^2 \text{ for } |i-j| \rightarrow \infty \tag{3.6}$$

This means that the correlations approach the magnetization squared for large distances. In our model, we use $i = L/4$ and $j = 3L/4$ as an approximation of the magnetization, to exclude the aforementioned boundary effects. The plot can be seen in Fig. 3.3. We can see a phase transition occuring at $g = 1$.

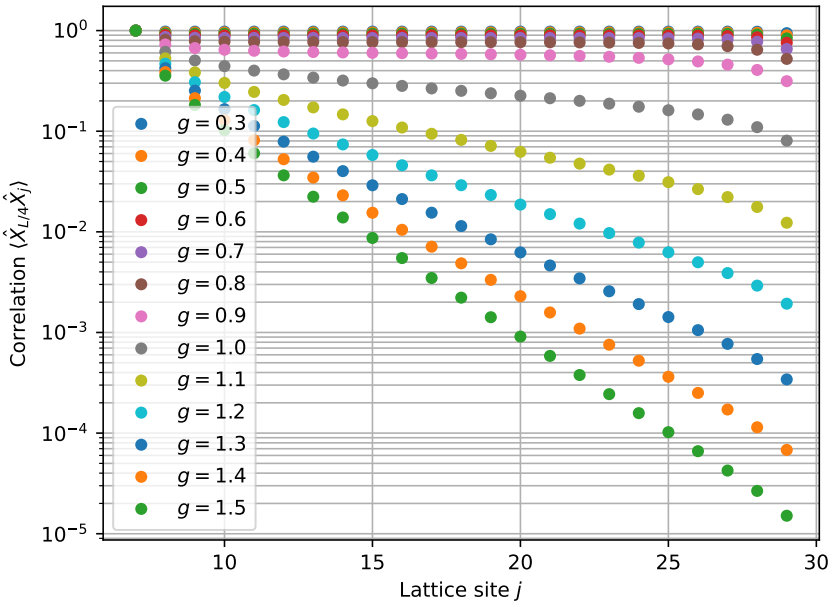

Figure 3.2: Correlations $\langle \hat{\sigma}_{x,L/4} \hat{\sigma}_{x,j} \rangle$ of the ground state of the Ising Hamiltonian against the lattice site j for different values of g on a logarithmic scale. We can see that for $g > 1$, the plots approach a linear function on the logarithmic scale.

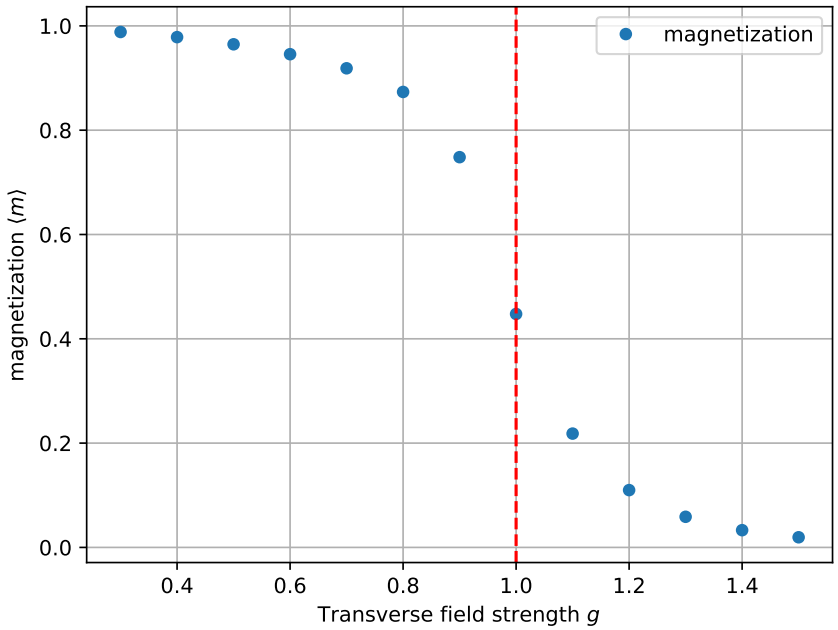

Figure 3.3: Magnetization of the system with respect to g. We can see a phase transition at $g = 1$.

3.4 Connected Correlations and Correlation Length

The connected correlations are defined as

$$C(j) = \langle \hat{\sigma}_{x,L/4} \hat{\sigma}_{x,j} \rangle - \langle \hat{\sigma}_{x,L/4} \rangle \langle \hat{\sigma}_{x,j} \rangle \tag{3.7}$$

This data can be seen in Fig. 3.4 Since the curve is linear in the logarithmic plot, we obtain data

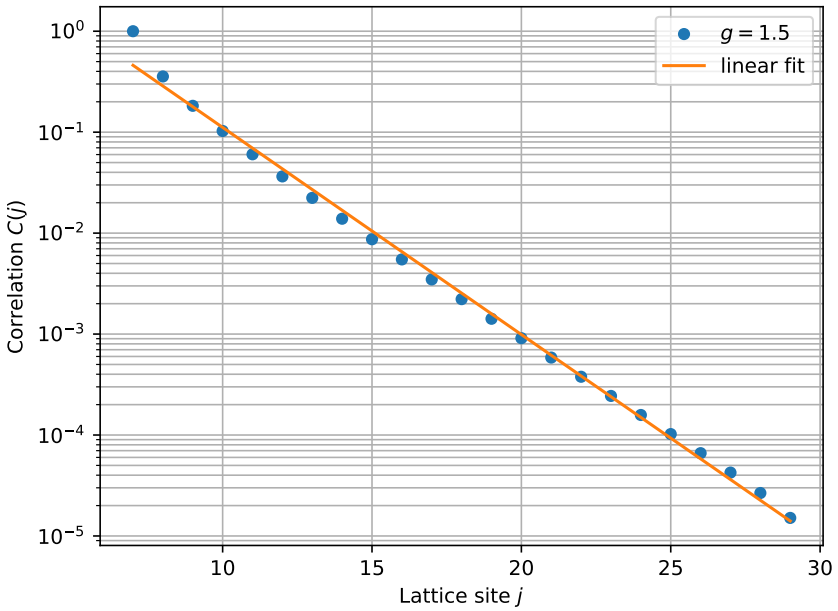

Figure 3.4: Linear fit in the logarithmic plot of the correlations. This can be used to extract the correlation length ξ.

of the kind

$$C(j) \propto \exp\left(-\frac{|j - L/4|}{\xi}\right) \tag{3.8}$$

We now use a linear fit of the logarithmic data

$$x = j \qquad\qquad y = \log\left(C(j)\right) \tag{3.9}$$

Therefore, we obtain 2 parameters a, b, that describe our fit-function

$$f(x) = a + bx = y \tag{3.10}$$

or according to our logarithmic fit:

$$C(j) = e^a \exp\left(bj\right) \tag{3.11}$$

Therefore, we can directly extract the correlation length ξ as

$$\xi = -1/b \tag{3.12}$$

Now, we want to take a look at the dependence of the correlation length on the strength of the external magnetic field, which strength is given by g. We therefore simulated a lot of additional ground states for different g values and extracted the correlation length through the linear fit, as shown exemplary in the section above. The obtained data is shown in Equation 3.4. One can clearly see that the correlation length converges to 0 for $g \to \infty$. This is in accordance to our expectation. In the case of a very large external fields, all spins are going to follow its direction. We therefore end up with a fully separable state, that has no correlation between the sites.

$$|\Psi\rangle_{\mathrm{GS},\, g\to\infty} = |\uparrow\rangle \otimes |\uparrow\rangle \otimes \cdots \otimes |\uparrow\rangle \tag{3.13}$$

This limit can also be seen in the plot.
Furthermore, we expect the correlation length to diverge at the critical point $g = 1$. This is not quite the case in our simulation. If we were to show the additional data for $g < 1$ it would look like an exponential decay starting at $g = 0$. This is due to the fact, that the divergence only happens in the thermodynamic limit, but we are only considering finite systems. Still, we can clearly see a large increase in the correlation length at the critical point $g = 1$.

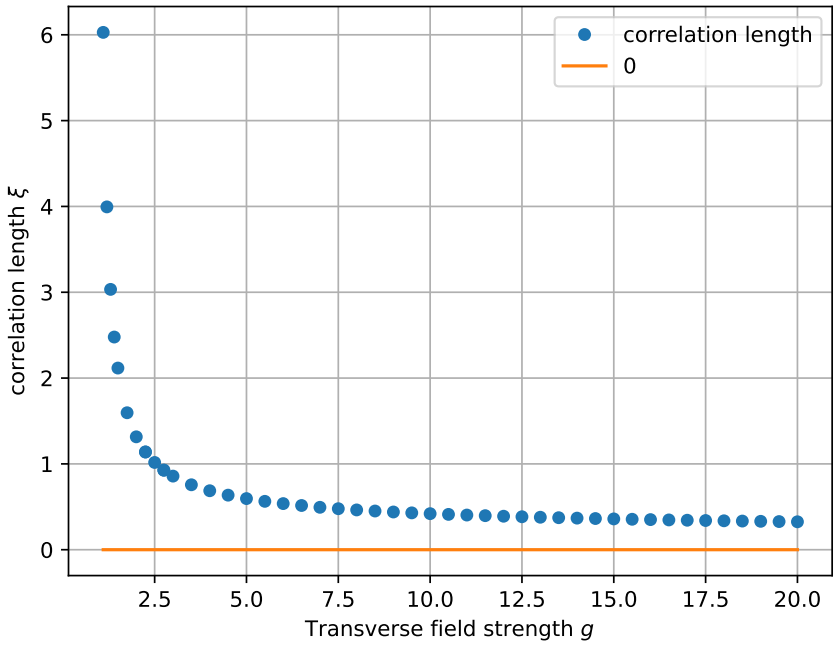

Figure 3.5: Visualization of the correlation length ξ with respect to g. One can see the steady decrease to $\xi \to 0$ for $g \to \infty$.

4 Day 2 – Time Evolution

4.1 Numerical specialties

The simulation of the real time evolution is going to take some time. Since we want to simulate different parameters, we are going to have to run this simulation over and over again. In order to speed up this procedure, we wrote GitHub automations. Those use multiple Ubuntu instances on GitHub servers and therefore can simulate a lot of different parameters in parallel. This speeds up the simulation time.

4.2 Entanglement

At first we are going to consider the time evolution of the on-site entanglement entropy. Plots for $g = 0.2$ and $g = 2$ can be found int Figure 4.1. In both cases we can see a similar behavior. We obtain a cone shaped evolution. We will consider the reflection on the boundary for $g = 2$ in the next part. This corresponds to an overall increasing entanglement entropy.

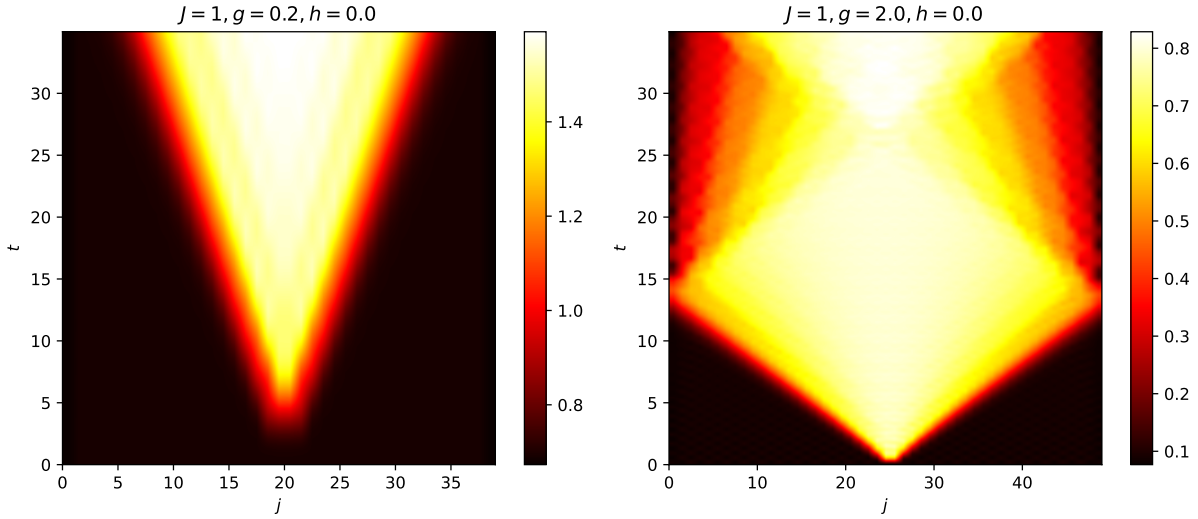

Figure 4.1: Time evolution of the entanglement entropy of the Ising chain for different system parameters.

Having a basically vanishing entanglement entropy at the start makes a lot of sense. At time $t = 0$ we are in the ground state of the Ising model. We use a MPS approach to simulate this

system. This approach is based on the fact of having quickly decreasing Schmidt coefficients, since we cut off those off at some point. Therefore having low entanglement at the start is in correspondence with our requirements for a stable numerical simulation.
If we let the system evolve, the sites will couple to each other, because of correlations between them. This leads to an increased entanglement, as can be seen in the plots.

4.3 Correlation

We now take a closer look at the correlations of the system. Here we can also see, that we start of with very localized correlations around our reference point at $L/2$. As the system evolves, those correlations spread out to the sides. We can see this in the form of "strings" rising to the top of the plot.
Those correlations also cause the increase of entanglement and therefore our observations are consistent within themselves.
Physically speaking, we insert an excitation at the spin at position $L/2$ in the system. This excitation can freely propagate and will do so. This can be seen by the fact, that the correlations grow out over time. In the $g = 2$ plot we can see something interesting. In this case, the excitation bounces off the wall. This is obviously not what we would expect in the real world, since this is only caused by the fact that we are limited to finite size systems. Nevertheless it is still really interesting to see, that the correlation does not vanish in noise, but we can still clearly see the reflected propagation.

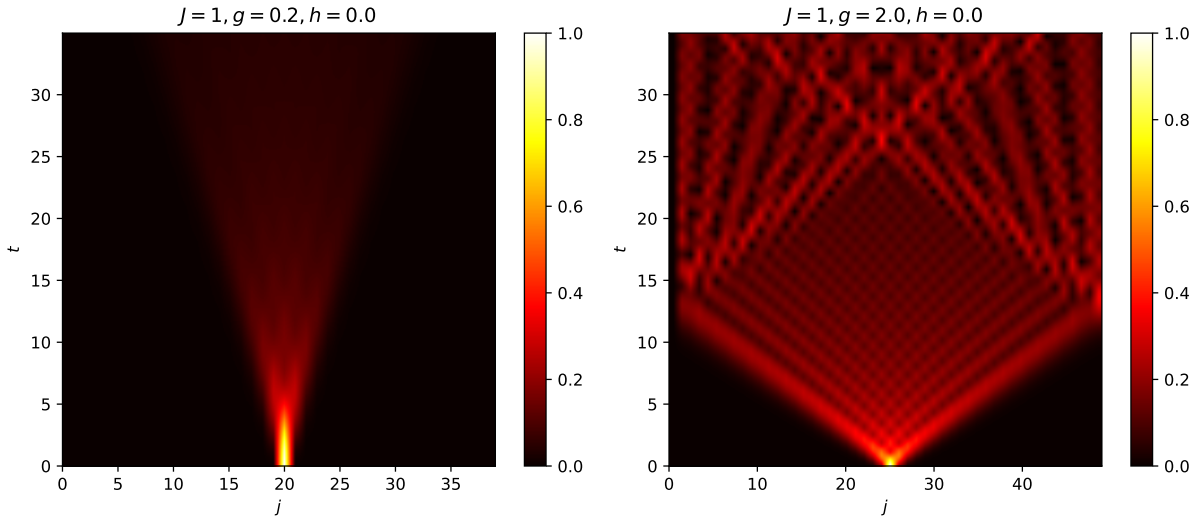

Figure 4.2: Time evolution of the correlations of the Ising model with different system parameters.

4.4 Dynamical Spin Structure Factor

Lastly we want to consider the spectrum of the system. This is an important quantity, especially with respect to experimental verification, since it can be measured in an experiment.
The spectrum is being obtained by the Fourier transform of the correlation.
First, we are going to neglect the longitudinal field by setting $h = 0$. In this case, we expect a gapless spectrum at the critical point $g = 1$, and a gap developing, as we go further away.
In the paramagnetic phase $g = 2$ we can recognize a cosine shaped plot, that has in fact a gap at $k = 0$. Therefore our results are consistent with our expectation.
In the ferromagnetic phase $g = 0.2$ we obtain a smeared out line, with the highest uncertainty at $k = 0$. Physically speaking, we now have 2 domain walls, that can propagate freely in the system. This causes the obtained spectrum.

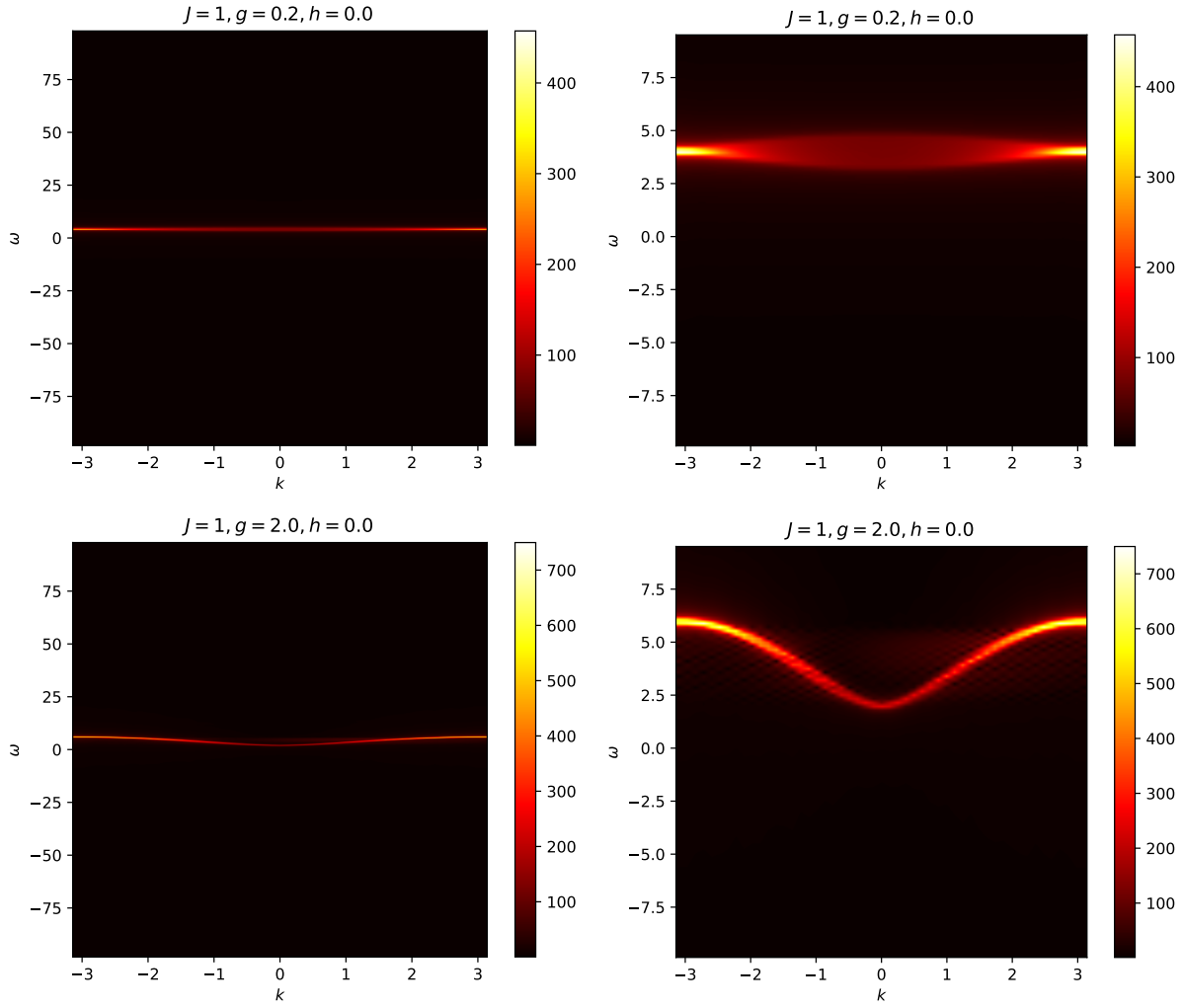

Figure 4.3: Spectrum of the Ising model for two different regimes $g = 0.2$ and $g = 2$. All plots horizontal next to each other show the same data, just with the right one being zoomed in a little bit.

If we now additionally consider a small longitudinal field $h = 0.1$, we can think of it as an confining potential. We therefore expect to trap the domain walls (those excitations are also called kinks).
Since we now have an longitudinal field, the spins have a preferred direction. If the domain walls move apart from each other, it requires an additional energy. Therefore the excitation with the lowest energy is just a single spin opposite of the favored direction. We can think of it like a bound state of pairs of kinks. Those bound states can be seen in the multiple excitations in the spectrum in Figure 4.4.

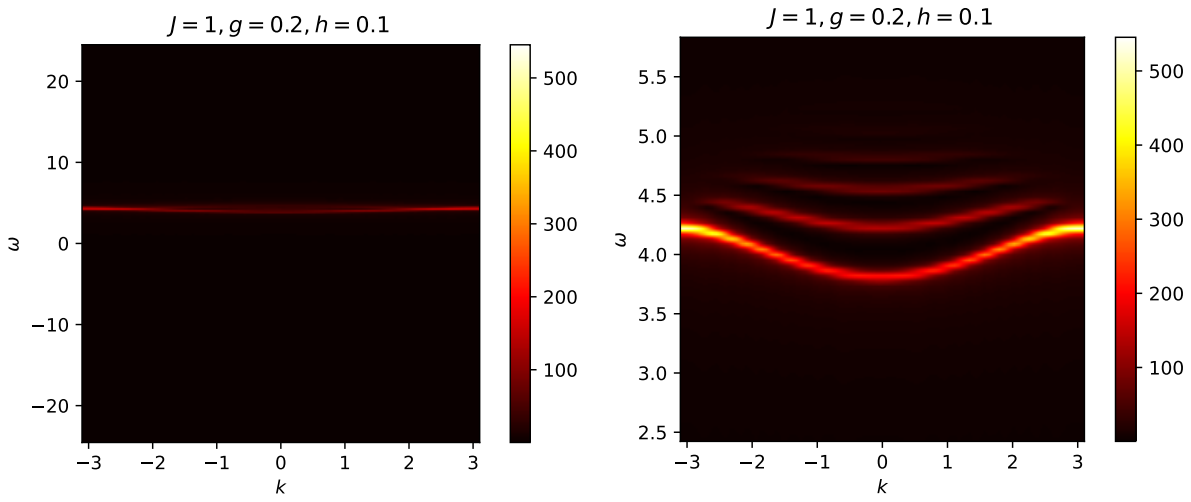

Figure 4.4: Spectrum of the Ising model with an additional field in z direction ($h = 0.1$). Both plots show the same data, just with the right one being zoomed in a little bit.

4.4.1 Comparison with the Roots of the Airy-function

In the last part we want to compare the maxima of our structure factor with the negative roots of the Airy function. This is sensible, since those negative roots are the solution of the corresponding Schrödinger equation [1].
In order to compare our results, we use the following relation, given in the solution

$$m_j = 2 \cdot m_0 + c \cdot z_j \tag{4.1}$$

where m_0 and c are constants and z_j are the negative roots of the Airy-function $Ai(-z_j) = 0$. Our results can be seen in Equation 4.4.1. If our simulation were in perfect unison with the theory, the maxima of the blue curve would be exactly at the red marks. As one can see, this is pretty much the case for the first 4 maxima, then our simulation starts to differ from the expectation.

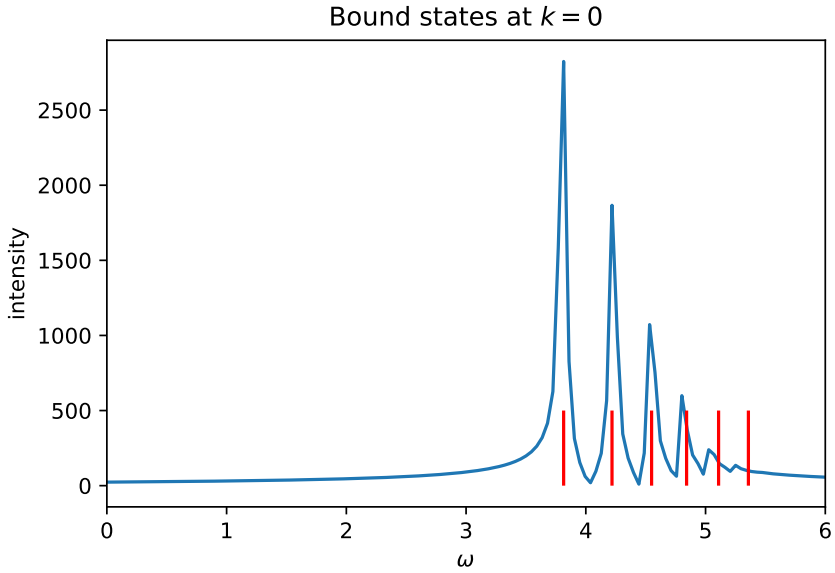

Figure 4.5: Comparison of the structure factor with the theoretical expectation. The horizontal red lines mark the negative roots of the Airy function scaled according to (4.1).

5 Conclusion

In this report, we used tensor networks methods to examine the behavior of 1D Ising chain Hamiltonian for medium-sized systems. In particular, these methods enabled the overcoming of the exponential scaling problem, which is common for numerical evaluation of quantum problems.
For the Ising chain, we were able to extract correlations between different sites, the magnetization and correlation length.
On day 2 we furthermore focused on the time evolution of the Ising model. We were able to identify the excitation and therein connected kinks. We therefore considered the time evolution of the correlations. There one could nicely see the outwards propagation for no longitudinal field and the confinement for an applied longitudinal field. We furthermore were able to show that our bound states are pretty close to the theoretical expectation - the negative roots of the Airy function.

6 Bibliography

[1] F. Pollmann, M. Drescher, and S. Lin, “Tensor-network simulations of bound states in perturbed quantum Ising chains”, 25 (2020), https://campus.tum.de/tumonline/LV_TX.wbDisplaySemplanDoc?pStpSplDsNr=21827 (visited on 06/06/2022).